Electron-ion-coincidence spectra of *K*-shell excited Ne, Ar, and Kr clusters

H. Murakami, K. Nagaya, Y. Ohmasa, H. Iwayama, and M. Yao
Department of Physics, Kyoto University, 606-8502 Kyoto, Japan

(Received 24 October 2006; accepted 7 December 2006; published online 6 February 2007)

Electron-ion-coincidence spectra were recorded for *K*-shell excited krypton, argon, and neon clusters covering the size range from 1 atom to about 3000 atoms by utilizing hard x-ray undulator beamlines. Multiply charged ions $R^{z+}(z \geq 2)$ and singly charged ions $R_n^+(n \geq 1)$ are observed as cluster fragments, and their relative abundance exhibits a characteristic dependence on the average cluster size $\langle N \rangle$. It is expected from these results that the charges generated on the cluster surface are strongly localized while those in the cluster core are more delocalized. The estimated charge separation distance increases with $\langle N \rangle$, and it is longer for lighter elements. © *2007 American Institute of Physics*. [DOI: 10.1063/1.2430706]

I. INTRODUCTION

Studies of clusters attract great interest as a link between atomic physics and condensed matter physics. Recently, core level excitation enables us to elucidate not only size-dependent but also site-dependent properties of clusters, and most of these studies have been devoted to rare-gas clusters by utilizing soft x rays emitted from synchrotron radiation sources.[1] When a core hole is generated within a neutral cluster by absorbing an x-ray photon, the cluster is changed to a multiply charged state by the Auger cascade decay, and then the charges are separated to different atomic sites within the clusters, resulting in the Coulomb explosion. In particular, fragmentation processes of $2p$-excited argon clusters have been well studied by coincidence experiments such as PIPICO,[2] PEPIPICO,[3] and PEPIPIPICO.[4] Here PE, PI, and CO are abbreviations for the photoelectron, the photoion, and the coincidence, respectively. Then, for example, PEPIPIPICO is an abbreviation for photoelectron-photoion-photoion-photoion-coincidence measurements. The *L*-shell excited Ar clusters become doubly or triply charged ions and then they will be dissociated into singly charged fragments being accompanied by considerable kinetic energy releases. The PEPIPICO results indicate both symmetrical and asymmetrical fission patterns as well as evaporation of neutral atoms from such ionized fragments.[3]

It is intriguing to study the physical properties of much more highly charged clusters. For this purpose, extending the core level excitation to deeper inner shell (i.e., *K* shell) by utilizing hard x rays is desirable, though the absorption cross section of hard x rays is considerably smaller compared with that of soft x rays. Although such multiply charged ions can also be produced by irradiation of ultrashort intense laser light[5] or by the collision of highly charged ions,[6] the core level excitation experiments may give complementary information on the deexcitation process because the excitation process is much simpler (i.e., one photon absorption) and the excited states are substantially localized.

Recently, Nagaya *et al.*[7] carried out electron-ion-coincidence (EICO) measurements for *K*-shell excited Kr clusters for the first time. The average number $\langle N \rangle$ of atoms within a cluster ranged from unity to about 1640. They found that the dominant ionic species stemming from small neutral clusters are highly charged monomer ions, while for medium size clusters singly charged monomer ions become the most abundant. Then the fraction of singly charged dimers and subsequently that of trimers increase with increasing cluster size. They have interpreted the characteristic size dependence of the relative abundance of daughter ions by assuming site-dependent decay processes as follows; when a core hole is generated in an atom located at the cluster surface, the holes deriving from the core hole due to the Auger cascade decay are strongly localized within the x-ray absorbing atom, while the charges are separated to surrounding atoms when the x-ray absorption takes place inside the cluster. Their observation is extremely interesting because it is consistent with the idea of interatomic Coulombic decay (ICD) which was theoretically predicted some years ago[8,9] and experimentally proven, recently.[10–13] However, it is only small Ne clusters and Ar dimers for which the validity of ICD has been established. Therefore, a systematic study for Ne, Ar, Kr, etc., is needed to discuss whether the ICD is applicable to various rare-gas clusters.

In the present study, we have taken the EICO spectra for *K*-shell excited neon and argon clusters covering the size range from a single atom to about 3000 atoms. The purpose of this paper is twofold. First, we make a systematic comparison of the EICO spectra among the various rare-gas clusters for the first time. Second, we discuss site-dependent localization or delocalization properties of charges in clusters, and furthermore evaluate the charge separation distance (CSD) in clusters.

II. EXPERIMENT

Neutral clusters were produced in a supersonic expansion of gas. We used cylindrical nozzles with a diameter of 80 μm for Kr and 60 μm for Ar and Ne. The nozzle was mounted on top of a cryostat which can be operated with liquid nitrogen. A gas jet created in an expansion chamber was introduced to an analyzing chamber through a conical skimmer with an aperture of 1 mm and crossed with the

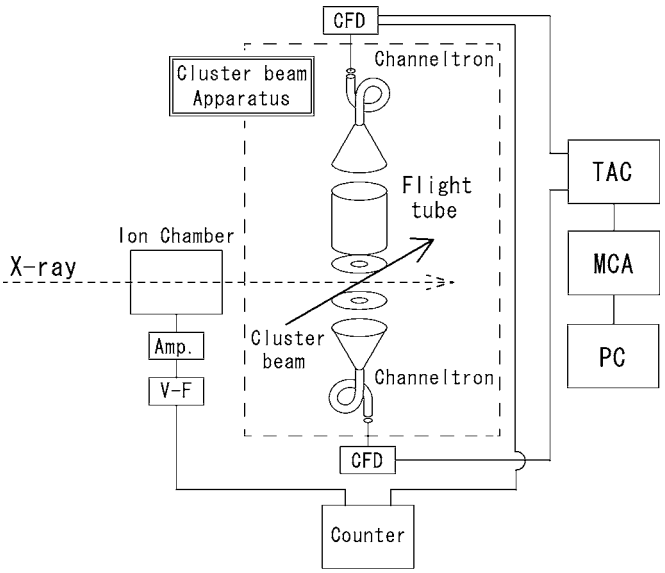

FIG. 1. A schematic drawing of the experimental apparatus for EICO measurements.

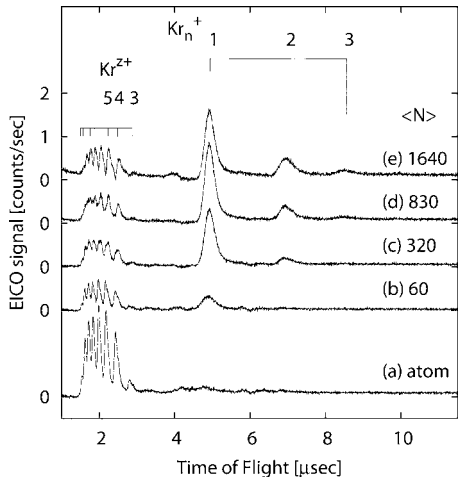

FIG. 2. EICO spectra for Kr (a) atom and [(b)–(e)] clusters. The average cluster sizes $\langle N \rangle$ are given in the figure. The x-ray energy was 14.50 keV, and the data accumulation time was 1800 s for each spectrum. In spectra (b)–(e), a contribution of uncondensed atoms in the cluster beam has been subtracted.

x-ray beam. The expansion chamber was evacuated by a turbomolecular pump with a pumping speed of 1500 l/s, and the analyzing chamber was pumped by another turbomolecular pump with 500 l/s. The pressure in the analyzing chamber was typically 10^{-4} Pa during the experiments.

The cluster size was varied by choosing appropriate expansion parameters: the stagnation pressure up to 15 bars, and the nozzle temperature down to 77 K for Ne, 130 K for Ar, and 150 K for Kr, respectively. The average cluster size was estimated from a mass spectrum obtained using electron impact ionization, and the result agreed well with a relation derived by Karnbach *et al.*[14] between the mass and the scaling parameter Γ^*.[15] As the starting materials of clusters, purchased rare gas with the purity of 99.999% was further purified by passing through a cold trap cooled with liquid N_2 for Ne gas and with dry ice immersed in ethanol for Ar and Kr.

The experimental setup is displayed in Fig. 1. The experiments for Kr clusters were carried out at the beamline BL10XU installed in SPring-8.[16] The details of the experiments were described elsewhere.[7] The experiments for Ar and Ne clusters were performed at the beamline BL37XU, where the high-brilliance x-ray emitted from the undulator was monochromatized by a Si(111) double crystal.[16] After passage through an ionization chamber filled with N_2 gas, the x-ray beam was led into the cluster beam apparatus through a beryllium window and crossed with the neutral cluster beam. The diameter of the cluster beam was about 10 mm in the photoionization range. The size of the x-ray beam was $0.5(V) \times 3(H)$ mm^2. The photon flux of the x-ray beam was about 3.6×10^{12} photons/s during our measurements. The measurements have been carried out at photon energies near the Kr K edge of 14.327 keV: 14.50 keV for Kr and 14.08 keV for Ar and Ne.

In our EICO measurements, ions were extracted by an entrance electrode (kept at −390 V), and they passed through a 215 mm long flight tube (kept at −2190 eV) and reached a detector (channeltron). The ion detection apparatus formed a Wiley-McLaren-type time-of-flight (TOF) mass spectrometer.[17]

The electrons were extracted by an entrance electrode (kept at 0 V) in the opposite direction and immediately detected by another channeltron. The electron signal, after passing a constant fraction discriminator (CFD) for noise reduction, was fed to a time-to-amplitude converter (TAC) as a start pulse, and the ion signal as a stop pulse. The TOF spectrum was recorded by a multichannel analyzer. In order to extract true EICO spectrum from raw data, we subtracted false-coincidence signals and a periodic time structure due to the bunch periodicity of the storage ring.

III. RESULTS

Figure 2 shows the EICO spectra of Kr atom (a) and clusters [(b)–(e)] with various sizes ($\langle N \rangle \leqslant 1640$). The data acquisition time was 1800 s for each spectrum. The raw data for these spectra are the same as those displayed elsewhere,[7] but in this case not only the background signals but also flat false-coincidence signals are subtracted. In contrast to the atomic spectrum (a), in which only multiply charged ions are seen, broad peaks due to the singly charged monomer, dimer, and trimer ions, Kr_n^+ ($n=1-3$), are observed above 4.5 μs in the spectra of clusters as well as a series of narrow peaks due to multiply charged monomer ions, Kr^{z+} ($z=3-11$). Here a contribution from uncondensed atoms was determined by mass spectrometry using electron impact ionization (EII) and subtracted from the EICO spectra. In the mass spectroscopy we counted the number of Kr^+ ions to know the fraction of uncondensed atoms, because Kr^+ is hardly produced by EII from clusters.[18] More details were written in the previous paper.[7] Note that multiply charged cluster ions such as Kr_n^{z+} ($n \geqslant 2$ and $z \geqslant 2$) are safely excluded, because such ions are not stable unless the ion sizes are sufficiently large.[19] Indeed no peaks corresponding to n/z=half integer is observed.

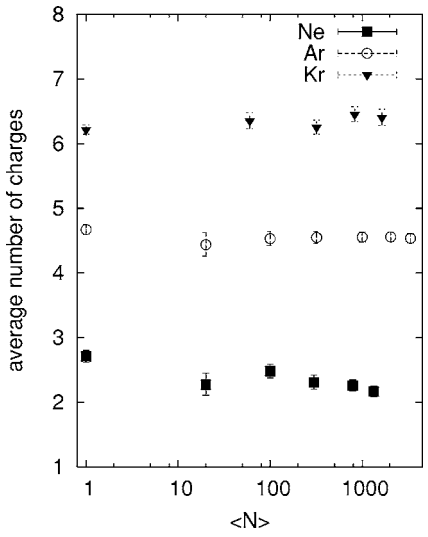

FIG. 3. Average number of charges for multiply charged ions is plotted as a function of $\langle N \rangle$. Statistical errors are denoted by bars.

No peaks due to the bigger cluster ions such as $n \geqslant 4$ were observed for the Kr clusters. The relative intensities of various multiply charged ions exhibit no appreciable size dependence. See also Fig. 3, where the average number of charges for the multiply charged ions is plotted as a function of the average cluster size $\langle N \rangle$.

Figure 4 shows the EICO spectra of Ar atom (a) and clusters [(b)–(g)] with various sizes ($\langle N \rangle \leqslant 3340$). For each spectrum, the counts were accumulated for 600 s, and both the background and constant false-coincidence signals were subtracted. The atomic spectrum includes the peaks due to the multiply charged monomers Ar^{z+} up to $z=8$ with a prominent central peak at $z=5$. The present spectrum differs from the daughter ion distribution with a central peak at $z=4$ obtained by Carlson and Krause,[20] but the reason for this discrepancy is quite simple. In the present experiment, the kinetic energy of the photoelectrons is so large (about 10.8 keV) that they cannot be detected efficiently as a start signal of TAC. The detection efficiency of the photoelectrons is estimated to be less than 15% from the geometry of our apparatus. Instead, the Auger electrons and shake-off electrons that have smaller kinetic energies mainly serve as the start signal. The distribution of multiply charged ions, that was accurately determined from a TOF mass spectrometry, can be well reproduced, when our spectrum is corrected for by using a prescription given by Krause and co-workers for Ne atoms.[21,22] In the present work, however, the EICO spectrum without such correction is employed as a standard, because 1*s* photoabsorption and Auger decay occur predominantly within a single atom,[23] that is, the detection efficiency does not change with cluster sizes. Indeed, the average number of charges remains nearly constant for Ar clusters (see Fig. 3). Furthermore, the shift of the central peak from $z=4$ to 5 is favorable for us to compare the deexcitation processes of Ar clusters with those of Kr clusters whose average z is 6.2.

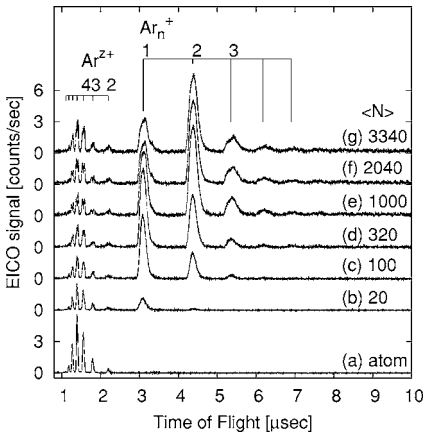

FIG. 4. EICO spectra for Ar (a) atom and [(b)–(g)] clusters. The x-ray energy was 14.08 keV, and the data accumulation time was 600 s for each spectrum. In spectra (b)–(g), a contribution of uncondensed atoms in the cluster beam has been subtracted.

In the EICO spectra of clusters [(b)–(g)], a series of narrow peaks due to multiply charged monomer ions, Ar^{z+} ($z=2-8$), is seen below 2.5 μs, and broad peaks due to the singly charged monomer of clusters, Ar_n^+ ($n=1-5$), are seen above 2.8 μs. Here a contribution from uncondensed atoms is subtracted from the EICO spectra using the same method as those for Kr clusters. The atomic fractions in the Ar cluster beams are about 0.5 for $\langle N \rangle = 20$ and about 0.2 for $\langle N \rangle \geqslant 100$. Compared with Kr clusters, larger fragments appear in the Ar cluster beam, though no other peaks such as Ar_n^+ ($n \geqslant 6$) were observed in the TOF range up to 10 μs. For small and medium size Ar clusters, the relative intensities of the Ar^+, Ar_2^+, and Ar_3^+ signals are comparable to those of Kr^+, Kr_2^+, and Kr_3^+ signals. However, the Ar_2^+, peak dramatically grows with further increasing $\langle N \rangle$, and eventually Ar_2^+, becomes an overwhelmingly dominant species for large clusters, and at the same time the relative abundance of the Ar^+ peak is reduced substantially. The dominance of Ar_2^+ was also found by Rühl *et al.* in their soft x-ray coincidence measurements[2–4] and *K*-shell excited PIPICO measurements with a size of $\langle N \rangle \sim 400$.[24] Furthermore, it should be noted that the peak shape changes remarkably with increasing $\langle N \rangle$. For small and medium size Ar clusters, each peak has a slightly asymmetrical shape with a tail on the longer TOF side. This shape is compatible with the Coulomb explosion: on the explosion, the faster ions that come towards the detector can be more efficiently detected than the slower ions that go in the opposite direction. For large Ar clusters, however, an additional peak centered at a slightly longer TOF seems to be superposed on the original peak, resulting in an apparent peak shift to a longer TOF. The additional peak may be assigned to such ions that were decelerated due to collisions with surrounding neutral atoms. As to the multiply charged ions, Ar^{2+} peak slightly grows with increasing $\langle N \rangle$.

Figure 5 shows the EICO spectra of Ne atom and clusters with various sizes ($\langle N \rangle \leqslant 1340$). The accumulation time was 600 s for each spectrum, from which the background and false-coincidence signals were subtracted. In the atomic spectrum the peaks corresponding to Ne^{z+} ions are seen up to $z=5$ with the most prominent peak at $z=3$, which is in good agreement with an early work.[21] In the spectra of clusters a series of narrow peaks due to multiply charged monomer ions, Ne^{z+} ($z=2-5$), is observed below 1.8 μs, and broad

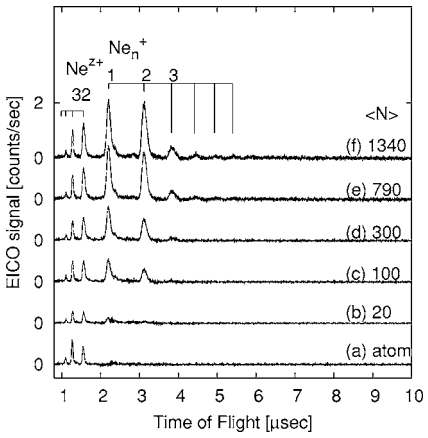

FIG. 5. EICO spectra for Ne (a) atom and [(b)–(f)] clusters. The x-ray energy was 14.08 keV, and the data accumulation time was 600 s for each spectrum. In spectra (b)–(f), a contribution of uncondensed atoms in the cluster beam has been subtracted.

peaks due to the singly charged monomer of clusters, Ne_n^+ $(n=1-6)$, are seen above 2.0 μs. Uncondensed atoms are subtracted, where the atomic fractions in the Ne cluster beams are about 0.7 for $\langle N\rangle=20$, 0.3 for $\langle N\rangle=100-300$, and 0.2 for $\langle N\rangle=790-1340$. The Ne_n^+ peaks grow with increasing $\langle N\rangle$, and the peak height of Ne_2^+ becomes comparable to that of Ne^+ at $\langle N\rangle=1340$. Unlike Ar clusters, the peak shape does not change appreciably even for large clusters. One characteristic feature for Ne clusters is that the Ne^{2+} peak grows with increasing $\langle N\rangle$ and becomes higher than that of Ne^+ at and above $\langle N\rangle=300$. Hence, the average number of charges in the multiply charged clusters decreases gradually with increasing $\langle N\rangle$, as shown in Fig. 3.

To summarize the experimental data, the relative abundance g_n of daughter ions, defined by Eq. (1), is shown as a function of $\langle N\rangle$ for krypton (a), argon (b), and neon (c) clusters in Fig. 6. For this purpose, we have estimated the abundance $A(n,Z=1)(\equiv A_n, n=1,2,3,\ldots,n_{\max})$ of singly charged ions R_n^+ by integrating the individual EICO peak. Here $n_{\max}$ is the number of atoms in the largest singly charged daughter ion: $n_{\max}=3$ for Kr and $n_{\max}=5$ for Ar and Ne clusters. For the multiply charged ions R^{z+} $(z\geqslant 2)$ the areas of all the relevant peaks are summed up, which gives $A(n=1,Z\geqslant 2)(\equiv A_0)$. To be precise, however, the detection efficiency r_n, which will be discussed below, has been corrected for $\tilde{A}_n=A_n/r_n$. Then the relative abundance g_n $(n=0,1,2,3,\ldots,n_{\max})$ is defined as

$$g_n=\tilde{A}_n \Big/ \sum_{k=0}^{n_{\max}} \tilde{A}_k. \tag{1}$$

The detection efficiency is limited by the probability $p_1^{(n)}$ of whether the photoions can reach the detector and the conditional probability $p_2^{(n)}$ of whether the photoions that have reached the detector can give a stop pulse to TAC.

An estimation of $p_1^{(n)}$ for various ionic species was made by simulating their Newtonian motion under a real geometry and applied voltages of the present detection system. For Kr and Ar clusters, the momentum distribution, which is taken as the initial condition of the equation of motion, was deduced from our recent multiple-ion-coincidence momentum imaging (MICMI) measurements.[25,26] For Ne clusters, for which MICMI data are not yet available, the full maximum at half width (FMHW) of the present EICO peaks was used. Generally, FMHW gives a bigger momentum distribution than MICMI measurements. We have found that all the ionic species, except for the singly charged monomers, can safely reach the detector. Thus, it is concluded that $p_1^{(n)}=1$ for $n\neq 1$, and that $p_1^{(1)}$ is 0.86 for Kr^+, 0.95 for Ar^+, and 0.98 for Ne^+.

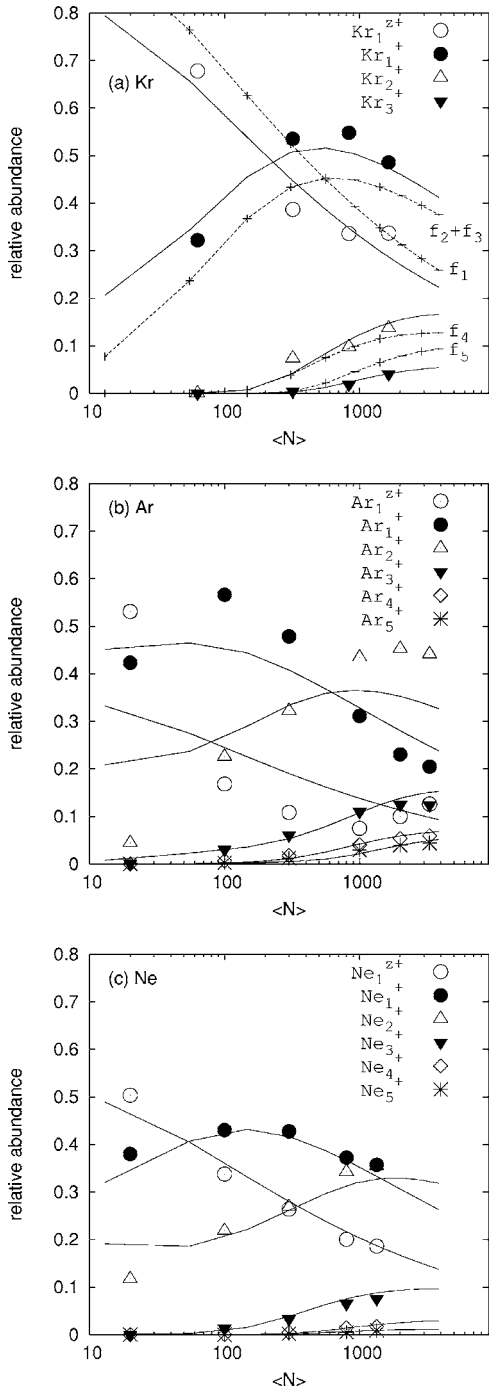

FIG. 6. Relative abundances of daughter ions are plotted for (a) Kr, (b) Ar, and (c) Ne clusters as a function of $\langle N\rangle$. The crosses in (a) denote the calculated fractions of atoms located in the lth outer layers of a perfect icosahedron, and the broken lines are their interpolations. The solid lines in (a)–(c) are the resulting fitting curves using Eq. (2).

In principle, $p_2^{(n)}$ should depend on the pulse-height distribution of the ion output pulses of the channeltron, and hence depend on the ion mass to charge ratio. In the present experiment, however, it has been confirmed that $p_2^{(n)}$ hardly depends on the ionic species, because the threshold voltage applied to CFD was far below the center of the pulse-height distribution. Thus, $p_2^{(n)}=p_2=$const. Then, setting $r_n=p_1^{(n)}p_2$, we obtain g_n.

Figure 6 reveals that the multiply charged ions are dominant for small clusters and their relative abundance decreases rapidly with increasing $\langle N\rangle$. The singly charged monomer ions have a broad maximum in the medium size range. The singly charged trimer and larger ions are very rare for small clusters and increase to an appreciable amount for large clusters. On the other hand, the behavior of the singly charged dimer ions depends on the element: the relative abundance of Kr_2^+ is negligibly small for small clusters and it remains about 10% even for large $\langle N\rangle$, while that of Ne_2^+ is more than 10% even for small $\langle N\rangle$ and increases gradually with $\langle N\rangle$. Finally, the relative abundance of Ar_2^+ increases rapidly to about 50%.

IV. DISCUSSION

In a previous paper,[7] we found that the relative abundance g_n of various daughter ions from Kr parent clusters has a close resemblance to the fraction f_l of atoms existing in the lth outer shell of icosahedrons. To be precise, the $\langle N\rangle$ dependence of g_0 resembles that of f_1; g_1 is similar to f_2+f_3, g_2 to f_4, and g_3 to f_5, as shown by the dashed lines in Fig. 6(a). It is expected from these results that, when the fragmentation occurs, the multiply charged monomer ions should derive from the cluster surface, the singly charged monomer ions from the interior of the cluster, and the singly charged dimer and trimer ions from the core of the cluster. These expectations are further supported by the following arguments.

First, it is well established experimentally and theoretically that in small rare-gas cluster ions there exists a trimer or tetramer ion core which behaves as a chromophore.[27–31] The chromophoric cores have linear conformations because of the directional character of the empty p orbital, and they are surrounded by neutral atoms that are arranged in rings or crowns. Second, charge localization on the cluster surface was proposed when multiple ionizations of Ar clusters were induced by a collision with highly charged Xe ions.[6] Third, we have carried out MICMI measurements for Kr (Ref. 25) and Ar (Ref. 26) clusters, and the major results from the experiment are as follows: (i) multiply charged ions are observed mainly for $N_{\mathrm{coin}}=1$, and hence only singly charged ions are observed for $N_{\mathrm{coin}}\geqslant 2$, N_{coin} being the number of coincident signals for each photodissociation event, and (ii) with increasing N_{coin} (i.e., with increasing the number of generated charges[25]), the average kinetic energy of singly charged monomer ions increases, while that of singly charged dimer and trimer ions decreases or remains small. The first result reveals that the multiply charged ions exhibit considerably different behavior from singly charged ions,[25] which is consistent with the site-dependent decay processes. Since the total Coulomb energy, which supplies the kinetic energy to the daughter ions, increases with the number of generated charges, result (ii) above looks contradictory. However, the apparent discrepancy can be removed by considering that the heavier ions are produced in the more central part of clusters where the Coulomb forces from the surrounding ions are more effectively canceled out due to the higher symmetry. Again, it is consistent with the suggested site dependence.

Thus, assuming the site-dependent decay processes, we will make further analysis of the $\langle N\rangle$ dependence of g_n for Kr, Ar, and Ne clusters by using the following equations:

$$\begin{aligned} g_0 &= a_{01}f_1 + a_{02}f_2 + \cdots + a_{0p}f_p, \\ g_1 &= a_{11}f_1 + a_{12}f_2 + \cdots + a_{1p}f_p, \\ g_2 &= a_{21}f_1 + a_{22}f_2 + \cdots + a_{2p}f_p, \\ &\vdots \\ g_k &= a_{k1}f_1 + a_{k2}f_2 + \cdots + a_{kp}f_p. \end{aligned} \tag{2}$$

Here the coefficients a_{nl} are fitting parameters, and the normalization conditions $\Sigma_{n=0}^{n_{\max}}a_{nl}=1$ are imposed. The initial values of a_{nl}, for example, for Kr clusters were $a_{01}=a_{12}=a_{13}=a_{24}=a_{35}=1$ (hereafter we will refer to these major terms as "diagonal") and other terms (i.e., "off-diagonal") were set to zero. Since the terms far from the diagonal are not important in the present case where the site dependence is assumed, they often remain zero even at the end of the fitting procedure. The solid lines in Fig. 6 are the resulting fitting curves, and the final values of a_{nl} are shown in Table I. For the Kr clusters the initial values are preserved to a great extent except for $l=5$, while for Ar and Ne clusters some of the diagonal terms are reduced to about one-half and the terms next to the diagonal get a finite value. The quality of fitting for Ar clusters is not so good compared with Kr and Ne clusters. The ambiguity is expressed as the standard deviation of the fit, S, in column 7 of Table I. Here S is the weighted sum of squared residuals divided by the number of degrees of freedom of the fit. The fitting results read as follows. When a surface Kr atom ($l=0$), for example, absorbs an x-ray photon, the atom changes into a multiply charged ion Kr^{z+} with a probability of 86% and changes into a singly charged monomer Kr^+ with a probability of 14%. See Fig. 7, where the decay processes in the fivefold icosahedral Kr cluster are schematically illustrated.

Since the normalization condition is imposed, the coefficients for each shell may be treated as branching ratios to various daughter ions in the fragmentation process. The average value of n on each shell, $\langle n(l)\rangle$, is listed at the bottom of each table part. In general, $\langle n(l)\rangle$ is nearly unity for the outer shells and increases with l. Comparing $\langle n(l)\rangle$ among the three elements, $\langle n(l)\rangle$ for Kr clusters is smaller than those for Ne and Ar clusters. The fact that the cluster ions such as dimers, trimers, etc., survived even after the Coulomb explosion strongly suggests that the electrons had been extended to several atoms.

TABLE I. Branching ratios of daughter ions produced in the *l*th outer shell of a cluster. Here, the structure of clusters is assumed to be a Mackey icosahedron. The average value of n on each shell, $\langle n(l)\rangle$, is listed at the bottom of each table part. The ambiguity of the fit is expressed as the standard deviation of the fit, S.

	l					
Product	1	2	3	4	5	S
Kr^{z+}	0.86	0	0	0	0	0.051
Kr^{+}	0.14	1	1	0	0	0.035
Kr_2^{+}	0	0	0	1	0.42	0.019
Kr_3^{+}	0	0	0	0	0.58	0.001
$\langle n(l)\rangle$	1.0	1.0	1.0	2.0	2.6	
Ar^{z+}	0.36	0	0	0	0	0.145
Ar^{+}	0.44	0.59	0	0	0	0.092
Ar_2^{+}	0.20	0.31	0.90	0.40	0	0.168
Ar_3^{+}	0	0.10	0.05	0.40	0.50	0.012
Ar_4^{+}	0	0	0.03	0.15	0.40	0.001
Ar_5^{+}	0	0	0.02	0.05	0.10	0.004
$\langle n(l)\rangle$	1.2	1.5	2.1	2.8	3.6	
Ne^{z+}	0.53	0	0	0	0	0.034
Ne^{+}	0.27	0.92	0	0	0	0.014
Ne_2^{+}	0.20	0.08	0.86	0.40	0.60	0.061
Ne_3^{+}	0	0	0.14	0.52	0.07	0.002
Ne_4^{+}	0	0	0	0.04	0.26	<0.001
Ne_5^{+}	0	0	0	0.04	0.07	<0.001
$\langle n(l)\rangle$	1.2	1.1	2.1	2.7	2.8	

The difference among the elements is more easily demonstrated by plotting the average number of atoms per charge, $\langle n\rangle$, calculated by

$$\langle n\rangle = \frac{\sum_{n=1}^{n_{\max}} nI_n}{\sum_{n=1}^{n_{\max}} I_n}, \tag{3}$$

where I_n is the integrated intensity of the peak in the EICO spectra. Here we neglect the multiply charged ions because they are not products during the Coulomb explosion. In Fig. 8 the average number of atoms per charge, $\langle n\rangle$, is plotted as a function of $\langle N\rangle$. Since the initial charges generated by 1*s* excitation are strongly localized, $\langle n\rangle$ can be regarded as a measure of a charge separation distance. Here $\langle n\rangle$ show a monotonous increase with $\langle N\rangle$ for all the elements. Compared among the rare-gas elements, $\langle n\rangle$ for Kr clusters is smaller than those of Ar and Ne clusters. In general, the chromophoric core exists in rare-gas cluster ions and its positive charge is more delocalized as the cluster size increases.[29–31] These works are limited for cluster size with several dozens, but Kuntz and Valldorf[29] speculated that more delocalized character would be expected for larger clusters.

We should still be careful in making a comparison among the elements, because there is a possibility that, even if stable ionic clusters are formed, they may be dissociated

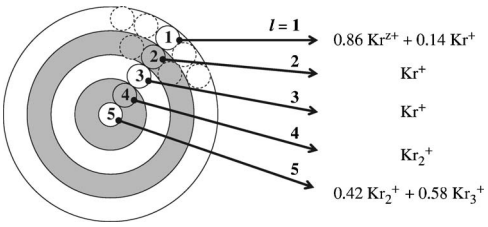

FIG. 7. Decay processes in the fivefold icosahedral Kr cluster are schematically illustrated. The daughter ions produced by the photoabsorption for the *l*th shell are shown on the right hand side (see Table I). When a surface atom absorbs an x-ray photon, it changes into a multiply charged ion Kr^{z+} with a probability of 86% and changes into a singly charged monomer Kr^{+} with a probability of 14%. On the other hand, when a central atom absorbs an x-ray photon, it changes into a singly charged dimer ion Kr_2^{+} with a probability of 42% and changes into a singly charged trimer ion Kr_3^{+} with a probability of 58%.

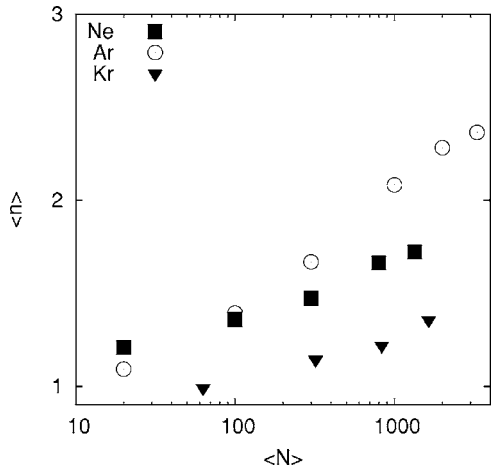

FIG. 8. Average number of atoms per charge, $\langle n\rangle$, is plotted as a function of $\langle N\rangle$ for Ne, Ar, and Kr clusters.

during the Coulomb explosion. Therefore, the observed $\langle n \rangle$ may be smaller than the average size of the stable ionic clusters before the Coulomb explosion. Nevertheless, one may conclude that Kr clusters have more localized character than the lighter elements, because the van der Waals potential of Kr is much deeper and hence Kr clusters are expected to be more stable.

Recently, Cederbaum *et al.*[8] proposed a novel type of electronic decay mechanism, ICD. In this process, the energy transfer by a virtual photon exchange can generate a hole in an adjacent atom. ICD is sensitive to the environment. Santra *et al.*[9] predicted theoretically that the Ne 2*s* lifetime strongly decreases with increasing number of neighbors in Ne clusters. Then, Öhrwall *et al.*[12] measured 2*s* lifetime in surface and bulk atoms of free Ne clusters. They reported that Ne 2*s* hole has a considerably longer lifetime for surface atoms than bulk atoms due to the fact that they have fewer nearest neighbors than bulk atoms. The ICD probability also depends on the distance D between the adjacent atoms as D^{-6}, which is similar to the dipole-dipole interaction. The present experiment reveals that the charges generated by core excitation are strongly localized on the surface and that CSD is longer for lighter elements. These results are, at least qualitatively, consistent with the ICD prediction.

V. CONCLUSION

The spectra of deep inner-shell excited rare-gas clusters were recorded by using the EICO technique. Multiply charged ions $R^{z+}(z \geqslant 2)$ and singly charged ions $R_n^+(n \geqslant 1)$ were observed for clusters, and their relative abundance exhibited a characteristic dependence on the average cluster size $\langle N \rangle$. It is expected from these results that the charges generated on the cluster surface are strongly localized while those in the cluster core are more delocalized, and heavier ions such as dimer and trimer ions are produced from the core of clusters. The CSD was estimated from the intensity distribution of the singly charged daughter ions. It is concluded that CSD increases with $\langle N \rangle$ and it is longer for lighter elements.

ACKNOWLEDGMENTS

The authors are grateful to H. Kajikawa and Y. Nishimori for their collaboration in carrying out experiments. This work is supported by the Grant-in-Aid for the 21st Century COE "Center for Diversity and Universality in Physics" from the Ministry of Education, Culture, Sports, Science and Technology (MEXT) of Japan. This work is also supported by the Grant-in-Aid for Scientific Research from the JPSJ (Nos. 12554013, 15651044, and 16201021).

[1] E. Rühl, Int. J. Mass. Spectrom. **229**, 117 (2003).
[2] E. Rühl, C. Schmale, H. W. Jochims, E. Biller, M. Simon, and H. Baumgärtel, J. Chem. Phys. **95**, 6544 (1991).
[3] E. Rühl, C. Heinzel, H. Baumgiirtel, M. Lavollee, and P. Morin, Z. Phys. D: At., Mol. Clusters **31**, 245 (1994).
[4] E. Rühl, A. Knop, A. P. Hitchcock, P. A. Dowben, and D. N. Mcilroy, Surf. Rev. Lett. **3**, 557 (1996).
[5] E. M. Snyder, S. A. Buzza, and A. W. Castleman, Jr., Phys. Rev. Lett. **77**, 3347 (1996).
[6] W. Tappe, R. Flesch, E. Rühl, R. Hoekstra and T. Schlathölter, Phys. Rev. Lett. **88**, 143401 (2002).
[7] K. Nagaya, M. Yao, H. Murakami, A. Mori, Y. Ohmasa, and H. Kajikawa, J. Phys. Soc. Jpn. **75**, 114801 (2006).
[8] L. S. Cederbaum, J. Zobeley, and F. Tarantelli, Phys. Rev. Lett. **77**, 4778 (1997).
[9] R. Santra, J. Zobeley, and L. S. Cederbaum, Phys. Rev. B **64**, 245104 (2001).
[10] S. Marburger, O. Kugeler, U. Hergenhahn, and T. Möller, Phys. Rev. Lett. **90**, 203401 (2003).
[11] T. Jahnke, A. Czasch, M. S. Schöffler *et al.*, Phys. Rev. Lett. **93**, 163401 (2004).
[12] G. Öhrwall, M. Tchaplyguine, M. Lundwall *et al.*, Phys. Rev. Lett. **93**, 173401 (2004).
[13] Y. Morishita, X. J. Liu, N. Saito *et al.*, Phys. Rev. Lett. **96**, 243402 (2006).
[14] R. Karnbach, M. Joppien, J. Stapelfeldt, J. Wörmer, and T. Möller, Rev. Sci. Instrum. **64**, 2838 (1993).
[15] O. F. Hagena and W. Obert, J. Chem. Phys. **56**, 1793 (1972).
[16] SPring-8 Users Office, *SPring-8 Beamline Handbook* (JASRI, Hyogo, 2004).
[17] W. Wiley and I. McLaren, Rev. Sci. Instrum. **26**, 1150 (1955).
[18] T. D. Märk, Int. J. Mass Spectrom. Ion Process. **79**, 1 (1987).
[19] O. Echt, D. Kreisle, E. Recknagel, J. J. Saenz, R. Casero, and J. M. Soler, Phys. Rev. A **38**, 3236 (1988).
[20] T. A. Carlson and M. O. Krause, Phys. Rev. **137**, A1655 (1965).
[21] M. O. Krause, M. L. Vestal, W. H. Johonston, and T. A. Carlson, Phys. Rev. **133**, A385 (1964).
[22] T. A. Carlson and M. O. Krause, Phys. Rev. **140**, A1057 (1965).
[23] T. Hayakawa, K. Nagaya, I. Yamamoto, Y. Ohmasa, M. Yao., and M. Nomura, J. Phys. Soc. Jpn. **69**, 2039 (2000).
[24] E. Rühl, C. Heinzel, A. P. Hitchcock, H. Schmelz, C. Reynaud, and H. Baumgärtel, J. Chem. Phys. **98**, 6820 (1993).
[25] H. Iwayama, K. Nagaya, H. Murakami, Y. Ohmasa, and M. Yao, J. Chem. Phys. (to be published).
[26] H. Murakami, H. Iwayama, K. Nagaya, Y. Ohmasa, and M. Yao, Eur. Phys. J. D (to be published).
[27] H. Haberland, B. Issendorff, T. Kolar, H. Kornmeier, C. Ludewigt, and A. Risch, Phys. Rev. Lett. **67**, 3290 (1991).
[28] T. Nagata and T. Kondow, J. Chem. Phys. **98**, 290 (1993).
[29] P. J. Kuntz and J. Valldorf, Z. Phys. D: At., Mol. Clusters **8**, 195 (1988).
[30] R. Kalus, I. Paidarova, D. Hrivnak, P. Paska, and F. X. Gardea, Chem. Phys. **294**, 141 (2003).
[31] P. Paska, D. Hrivnak, and R. Kalus, Chem. Phys. **286**, 237 (2003).